

# The impacts of net long-wave radiation on the surface soil thermal regimes over the Qinghai–Tibetan Plateau, China

Ren Li<sup>1</sup> · Lin Zhao<sup>1</sup> · Tonghua Wu<sup>1</sup> · Xiaodong Wu<sup>1</sup> · Yao Xiao<sup>1</sup> · Yizhen Du<sup>1</sup> · Yanhui Qin<sup>1</sup>

Received: 11 October 2014 / Accepted: 28 July 2015 / Published online: 25 January 2016  
© Springer-Verlag Berlin Heidelberg 2015

**Abstract** Radiation data measured at six stations on the Qinghai–Tibetan Plateau (QTP) were used to analyze the variation of net long-wave radiation ( $L_n$ ). The stations were located in the arid, semiarid, and sub-humid climate zones, covering the major climate types of the QTP. The impacts of  $L_n$ , combined with soil temperature data, on the thermal regime of ground surfaces were evaluated.  $L_n$  varied regionally over the QTP. It decreased in the northeastern and western parts and the interior of the QTP, while it showed an increasing trend in the southeastern part of the QTP.  $L_n$  declined significantly at a rate of  $0.415 \text{ MJ m}^{-2} \text{ day}^{-1}$  per decade during the past 20 years.  $L_n$  greatly influenced the freezing index (DDF). DDF and the surface freezing–thawing intensity (FTI) increased with decreasing  $L_n$ .  $L_n$  was negatively correlated with FTI and this was most pronounced with a 2-year-lag FTI. The ratio of  $L_n/R_s$  ( $R_s$  denotes the global radiation) was greater than the surface albedo ( $R_k/R_s$ ) ( $R_k$  denotes the reflected radiation). Both parameters resulted in surface energy loss and a lowering of the surface temperature. The cooling effect of  $L_n/R_s$  exceeds that of  $R_k/R_s$ .

**Keywords** Net long-wave radiation · Soil thermal regime · Freezing–thawing intensity · Qinghai–Tibetan Plateau

## Introduction

Surface net long-wave radiation ( $L_n$ ) represents the difference between the upward long-wave radiation emitted from the surface and the downward long-wave radiation from the atmosphere. It is the quantity of heat loss from the ground surface through  $L_n$  exchange (Zhou et al. 1990). The magnitude of  $L_n$  is influenced by surface temperature, humidity, and cloud cover (Iziomon et al. 2001; Prata 2008; Allan 2009; Philipona et al. 2009; Wang and Liang 2009; Zhang et al. 2010), and it is a useful parameter for predicting surface minimum temperature and frost.

The thermodynamics of the Qinghai–Tibetan Plateau (QTP) plays an important role in the East Asian climate system. The magnitudes of  $L_n$  and net radiation in this region are similar and they influence surface and atmospheric heating (Zhou 1984a, b; Ji et al. 1986, 1987). The study of  $L_n$  is an important area of atmospheric research. Previous studies of  $L_n$  in China, limited by the lack of sophisticated instrumentation, typically used radiation graphic methods or empirical and semi-empirical formulas (Zuo et al. 1965; Gao and Lu 1982). Previous radiation graphics methods used a variety of technologies. Calculated values often differed significantly and these calculations could only be performed using data obtained from regions with permanent stations (Zhou et al. 1964). With the launch of the QTP Meteorological Scientific Experiment (QXPME) in 1979, the  $L_n$  is now obtained using direct measurement rather than from calculations (Ji et al. 1987).

Long-wave radiometers in China are now common and the large amount of new data allows detailed study of  $L_n$ . The data, including the distribution and variation of  $L_n$ , parameterization schemes, and satellite observations have been extensively documented (Zhou 1984a, b; Weng and

✉ Tonghua Wu  
thuawu@lzb.ac.cn

<sup>1</sup> Cryosphere Research Station on the Qinghai–Tibet Plateau, State Key Laboratory of Cryospheric Sciences, Cold and Arid Regions Environmental and Engineering Research Institute, Chinese Academy of Sciences, Lanzhou 730000, China

Feng 1984; Weng et al. 1984; Ji 1985; Ji et al. 1987, 1989; Li et al. 2006).  $L_n$  values are relatively high in the QTP area of China (Sun and Weng 1986) and, within the QTP,  $L_n$  values are greater in the western than in the eastern part (Ji et al. 1987). In the radiative balance equation, the ratio of  $L_n$  to global radiation ( $R_s$ ) is larger than that of the reflected radiation ( $R_k$ ) to  $R_s$ . Therefore, in the study of QTP land-surface processes and simulation of global changes, an important factor is the effect of  $L_n$  variation on climate caused by changes in condition of the ground surface (Ji et al. 1995, 1996, 1997; Ji 1997, 1998, 1999, 2003). A comprehensive understanding of the characteristics of  $L_n$  and its role in the land-atmosphere physical processes is possible. However, availability of time series data is meager. Existing data mostly focus on description of the characteristics of  $L_n$  over the QTP, analysis of factors affecting  $L_n$ , and the selection of optimal parameterization schemes. Less work has been done on the role of  $L_n$  in the heat exchange between the ground surface and the atmosphere. Thorough study of the variability of  $L_n$  and its effects on the thermal characteristics of the ground surface will contribute to understanding the response of frozen soil to climatic change.

The objective of this study was to analyze the characteristics of  $L_n$  and its effects on the thermal regimes of the ground surface.  $L_n$  data were obtained at Wudaoliang (WDL), Xidatan (XDT), and Tanggula (TGL). Radiation balance data were obtained at Golmud (GLM), Shiquanhe (SQH), and Changdu (CD). Surface soil temperature data were used to evaluate the relationship between  $L_n$  and the freeze-thaw intensity (FTI) over the QTP as well as its relationship to the cumulative soil temperature during the freezing period. The ratios of  $L_n$  and  $R_k$  to  $R_s$  are considered as factors whose variations influence the surface soil temperature.

## Data and methods

Global radiation  $R_s$  (0.28–3.0  $\mu\text{m}$ ) and reflected radiation  $R_k$  (0.28–3.0  $\mu\text{m}$ ) were measured at WDL from 1993 to 2002, using an MS-42 radiometer (EKO, Japan). Long-wave radiation  $L_n$  (3.5–50.0  $\mu\text{m}$ ) was measured with a high-resolution Eppley Precision Infrared radiometer (Newport, Rhode Island, USA). All output data were recorded on a DT600 data logger (Esis Pty. Ltd., Australia) and sampled each hour with reference to local time (1 h 48 min behind Beijing standard time). Corresponding observations were carried out using a CNR-1 net radiometer with a wavelength range from 0.3 to 3.0  $\mu\text{m}$  in the short-wave band, and from 3.5 to 50.0  $\mu\text{m}$  in the long-wave band (Kipp & Zonen Co., Delft, The Netherlands). Data were recorded with a CR23X data logger (Campell

Scientific Corp., Edmonton, Alberta, Canada). Radiation observations at TGL and XDT were also made with CNR-1 net radiometers, as described in Zhao et al. (2008). Radiation data at GLM, SQH, and CD were obtained from the Annual Solar Radiation Data of China published by the National Climate Center of China. Meteorological data at TGL and XDT were obtained from measurements made at the Cryosphere Research Station on the Qinghai-Tibet Plateau, and meteorological data at WDL, GLM, SQH, and CD were obtained from the Annual Surface Meteorological Data of China published by the National Climate Center of China.

All sensors were calibrated at the beginning and end of the experiments with regular maintenance conducted by the Chinese Academy of Meteorological Sciences at 2-year intervals. Calibration results at WDL showed that the relative errors of short-wave radiation were <5 % and the relative errors of long-wave radiation were <4 %. Net long-wave radiation values were obtained as the difference between the upward and downward long-wave radiation. The observation uncertainty of these values was estimated using the square root of the sum of the individual upward and downward long-wave radiation uncertainties. The  $L_n$  uncertainty, using this procedure, was <5.7 % (Jacovides et al. 1993; Niemelä et al. 2001).

Observations of the surface energy balance in China were initiated at solar radiation stations in January 1993, but long-wave radiation observations were not made at that time. The  $L_n$  at a solar radiation station can be determined from components of the radiation balance observations using the following method. The surface radiation balance equation, during the day, is:

$$R_{n,\text{day}} = R_s - R_k - L_{n,\text{day}} \quad (1)$$

At night, when short-wave radiation is absent, the radiation balance equation becomes:

$$R_{n,\text{night}} = -L_{n,\text{night}} \quad (2)$$

Adding Eqs. (1) and (2) gives:

$$R_n = R_s - R_k - L_n \quad (3)$$

in which  $R_{n,\text{day}} + R_{n,\text{night}} = R_n$  and  $L_{n,\text{day}} + L_{n,\text{night}} = L_n$ , where  $R_{n,\text{day}}$  and  $R_{n,\text{night}}$  are the net radiation during the day and at night, respectively.  $L_{n,\text{day}}$  and  $L_{n,\text{night}}$  are the values of  $L_n$  during the day and at night, respectively. In Eq. (3),  $R_s$  is incoming radiation energy,  $R_k$  and  $L_n$  are the short-wave and long-wave radiation energy loss, respectively. Given  $R_n$ ,  $R_s$ , and  $R_k$ , then  $L_n$  can be expressed as:

$$L_n = R_s - R_k - R_n \quad (4)$$

From Eq. (4), we obtained the  $L_n$  values at GLM, CD, and SQH. To extend the  $L_n$  data series of the WDL station, the method proposed by Li et al. (2006) was used. The

method estimated  $L_n$  using disturbance quantities caused by different meteorological elements related to its mean value. The results of  $L_n$  using the proposed method agreed with the measured values at Naqu, Ganzi, Lhasa, Gezei, and WDL within the QTP. The absolute error was  $3.6 \text{ W m}^{-2}$  and the relative error was 4 %. Additionally, measurements performed at WDL from 1998 to 2000 (not used in the method construction) were used for validation of the proposed method. Verification results showed good agreement between the measured and estimated  $L_n$  values. The values of absolute error and relative error were  $5.2 \text{ W m}^{-2}$  and 6.3 %, respectively. This confirmed that the proposed model adequately predicts  $L_n$  values and that this method can be used for estimation of  $L_n$ . We obtained  $L_n$  values at the WDL from January 1977 to August 1993 and from January 2003 to December 2004.

Ground surface (at 5 cm depth) temperature data from 74 meteorological stations were collected to analyze the thermal state of the ground surface. Surface freezing index (DDF) and surface thawing index (DDT) were calculated by the methods of Frauenfeld et al. (2007) and Wu et al. (2011). When the daily mean temperature at 5 cm depth at different stations consistently remained below  $0 \text{ }^\circ\text{C}$ , calculation of DDF began. When the daily mean temperature consistently remained above  $0 \text{ }^\circ\text{C}$ , DDT calculations were initiated. The number of freezing days at various stations was recorded as FDN (number of days with below  $0 \text{ }^\circ\text{C}$  soil temperature values at 5 cm), and the number of thawing days was recorded as TDN (the number of days with above  $0 \text{ }^\circ\text{C}$  soil temperature values at 5 cm). The cumulative temperature during the freeze–thaw period determines the freeze–thaw intensity (FTI) which can be calculated using the following equation (Nelson and Outcalt 1987):

$$\text{FTI} = \frac{\sqrt{\text{DDT}}}{\sqrt{\text{DDT}} + \sqrt{\text{DDF}}} \quad (5)$$

## Results and discussion

Sensible heat and latent heat both have significant effects on positive surface temperatures, but  $L_n$  variations have an important influence on lowering surface temperatures (Zhou et al. 2000). For example, soil freezing occurs when the  $L_n$  is greater than the absorbed radiation. When net radiation has a consistent negative value, the surface temperature decreases to below  $0 \text{ }^\circ\text{C}$  (Zhou et al. 2000).

### $L_n$ variability in different QTP regions

Among six QTP stations, the  $L_n$  data time series was relatively longer at GLM ( $36^\circ 25' \text{N}$ ,  $94^\circ 54' \text{E}$ , 2809.2 m a.s.l.),

CD ( $31^\circ 09' \text{N}$ ,  $97^\circ 10' \text{E}$ , 3307.1 m a.s.l.), SQH ( $32^\circ 30' \text{N}$ ,  $80^\circ 05' \text{E}$ , 4279.3 m a.s.l.), and WDL ( $35^\circ 13' \text{N}$ ,  $93^\circ 05' \text{E}$ , 4614.2 m a.s.l.). The beginning observation dates of  $L_n$  at these four stations are similar. Therefore,  $L_n$  data from the four QTP stations were used to analyze  $L_n$  variation in the Gobi desert region in the northeast, the relatively humid southeast region, the arid west desert region, and the alpine frost desert steppe region. Detailed study site locations are shown in Fig. 1. GLM, CD, and SQH sites are in a region of seasonally frozen ground, with maximum frozen depth (MFD) of about 114, 62, and 46 (Li et al. 2009), respectively. WDL is located in the continuous permafrost region with an active layer thickness (ALT) of about 220 cm (Li et al. 2012).

Figure 2 shows  $L_n$  values for different regions of the QTP. GLM and SQH are in the northeastern and western arid regions of the plateau, CD is in the eastern sub-humid region of the plateau, and WDL is in the sub-frigid and semiarid region of the plateau (Zheng et al. 1979). In the northern arid region (Fig. 2a), the annual mean  $L_n$  at GLM ranged from  $7.97$  to  $10.25 \text{ MJ m}^{-2} \text{ day}^{-1}$ , with a mean of  $9.18 \text{ MJ m}^{-2} \text{ day}^{-1}$  over the period 1993–2012. Large values of  $L_n$  occurred in 2007 while a relatively small value occurred in 2012. The variation in amplitude of the time series was about  $2.28 \text{ MJ m}^{-2} \text{ day}^{-1}$ . During the past 20 years,  $L_n$  decreased at a rate of  $0.511 \text{ MJ m}^{-2} \text{ day}^{-1}$  per decade at this region. In the study period, the mean annual precipitation increased by 11.0 mm per decade. The water vapor pressure increased at a rate of 0.11 hPa per decade. Water vapor in the air is effective at absorbing upward long-wave radiation (Prata 2008; Allan 2009; Philipona et al. 2009; Wang and Liang 2009). Because of this, a relative increase in downward long-wave radiation occurs leading to decreased  $L_n$ . The magnitude of  $L_n$  fluctuation at GLM is closely related to the characteristics of the local climate and the ground surface. It reflects the variation characteristics of  $L_n$  in the arid northeast QTP climatic zone.

Annual mean  $L_n$  at SQH ranged from 11.70 to  $19.19 \text{ MJ m}^{-2} \text{ day}^{-1}$ , with a mean value of  $14.30 \text{ MJ m}^{-2} \text{ day}^{-1}$  in the arid western region (Fig. 2c). In the  $L_n$  series, a maximum  $L_n$  value occurred in 1995 while a minimum value occurred in 2010. The variation amplitude in this region was about  $7.49 \text{ MJ m}^{-2} \text{ day}^{-1}$ . Figure 2c shows that  $L_n$  in this region had a decreasing trend. During the past 20 years,  $L_n$  decreased by  $1.048 \text{ MJ m}^{-2} \text{ day}^{-1}$  per decade. From 1995 to 2012,  $L_n$  decreased by  $7.49 \text{ MJ m}^{-2} \text{ day}^{-1}$ . The decrease in  $L_n$  at SQH was related to regional precipitation. Mean annual precipitation at SQH is 65 mm but annual precipitation ranged from 25 to 120 mm. Precipitation at SQH increased at a rate of 6.2 mm per decade and the atmospheric humidity has increased from 1995 to 2012. Atmospheric

**Fig. 1** The locations of study sites on the Qinghai–Tibetan Plateau

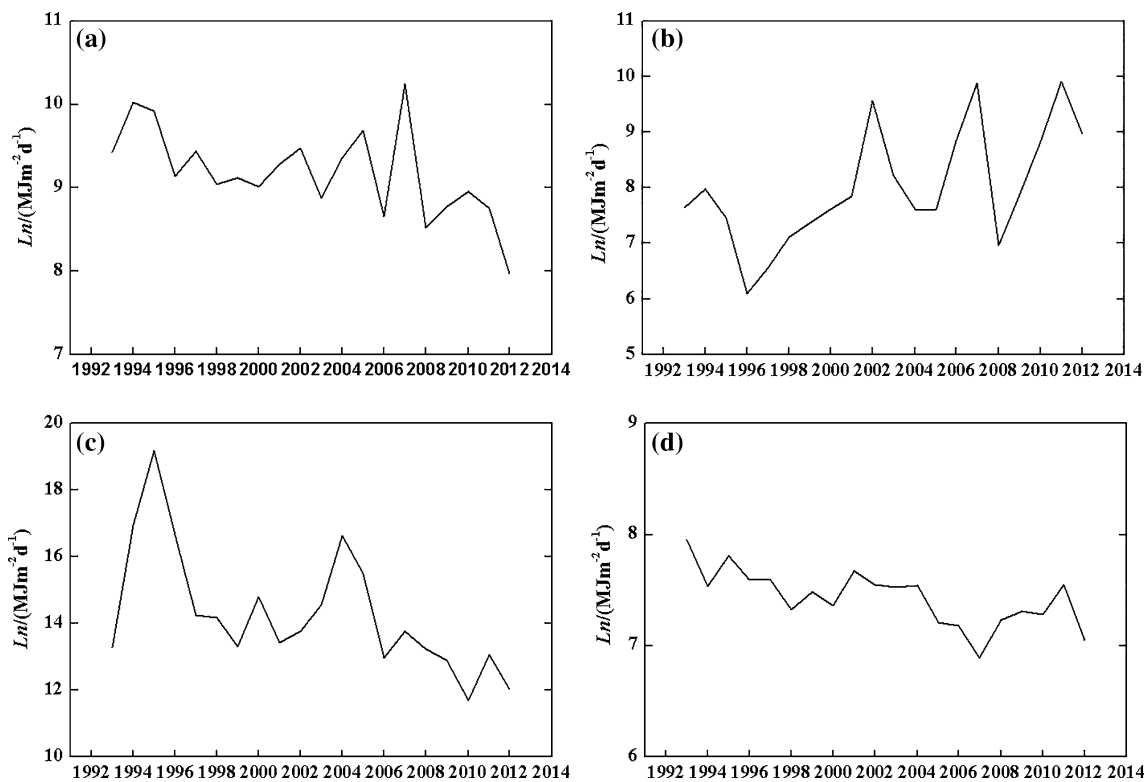
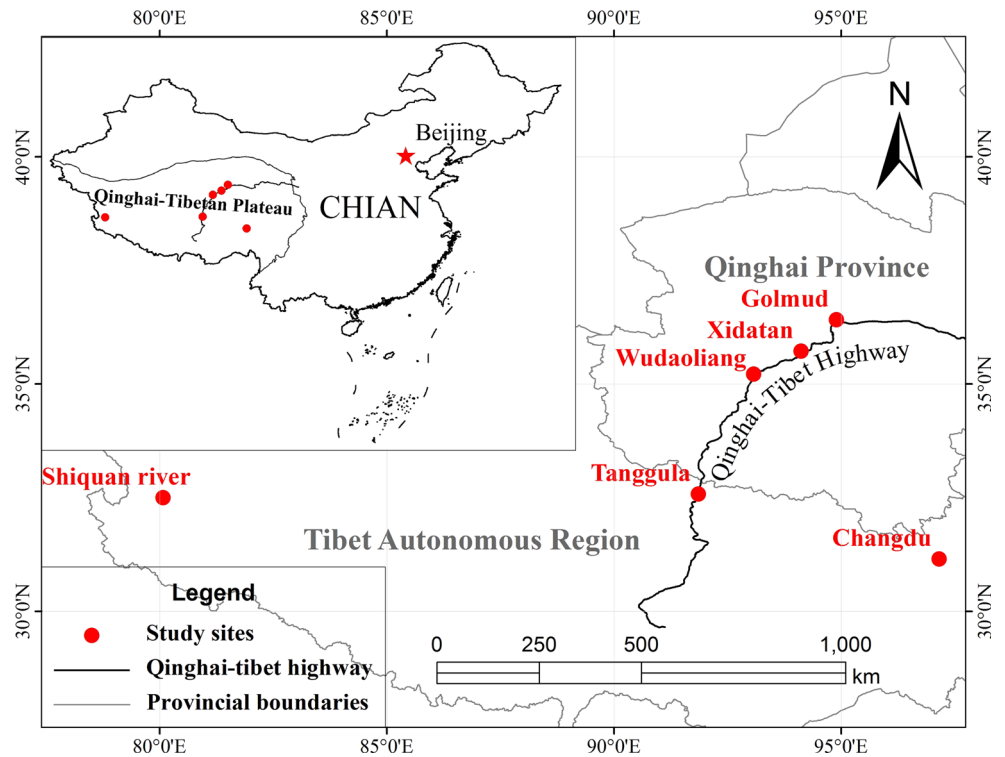


**Fig. 2** Spatial variations of  $L_n$  in different regions of the Qinghai–Tibetan Plateau

water vapor strongly absorbs long-wave radiation and can increase atmospheric counter-radiation (Prata 2008; Allan 2009; Philipona et al. 2009; Wang and Liang 2009). Thus,

significant  $L_n$  variation was linked to increased variation in annual precipitation. Other work has documented a significant increase in low-level clouds during the nights over

the QTP from 1961 to 2003. This resulted in enhanced atmosphere counter-radiation which weakened the  $L_n$  (Dun and Wu 2006).

At WDL (Fig. 2d),  $L_n$  had a temporal variation pattern similar to the northern and western arid regions. The annual mean  $L_n$  at WDL ranged from 6.89 to 7.95 MJ m<sup>-2</sup> day<sup>-1</sup>, with a mean of 7.43 MJ m<sup>-2</sup> day<sup>-1</sup>. The regional  $L_n$  series fluctuated but continuously decreased from 1993 to 2012 at a rate of 0.297 MJ m<sup>-2</sup> day<sup>-1</sup> per decade. The  $L_n$  at TGL (southwest of WDL) during 2005 to 2008 also had a decreasing trend. The  $L_n$  at Hebei alpine meadow in the Qilian Mts (northeast part of QTP) had a similar decreasing trend (Zhang et al. 2010). Other studies (Ji et al. 1987; Nelson and Anisimov 1993; Iziomon et al. 2001; Prata 2008; Allan 2009; Philipona et al. 2009; Wang and Liang 2009; Zhang et al. 2010; Wacker et al. 2011) found that the long-wave radiation exchange was mainly affected by air temperature, cloud cover, water vapor, and atmospheric aerosol levels. In the WDL region, clouds and rainfall have significant influence on long-wave radiation (Ji et al. 1987, 1995). Atmospheric quality is another factor affecting  $L_n$ . The influence of aerosols on  $L_n$  indicated that the Angstrom turbidity coefficient  $\beta$  (Li et al. 2005) and the surface  $L_n$  had an inverse relationship. This results from aerosol particulates absorbing long-wave radiation. The presence of aerosol particulates in the atmosphere increases the downward long-wave radiation. In addition, aerosol particulates act as condensation nuclei for clouds. Particulates absorb water vapor to stimulate cloud formation (Ruckstuhl et al. 2008). Aerosol particulates alter the micro-physical and radiation characteristics of clouds and lead to a decrease of long-wave radiation.

The annual mean  $L_n$  at CD in the sub-humid region of eastern QTP ranged from 6.10 to 9.91 MJ m<sup>-2</sup> day<sup>-1</sup>, with a 20-year mean of 7.80 MJ m<sup>-2</sup> day<sup>-1</sup> (Fig. 2b). A maximum value of  $L_n$  was recorded in 2011 while a minimum value occurred in 1996. The variation amplitude in the time series was 3.81 MJ m<sup>-2</sup> day<sup>-1</sup>. Compared with arid and semiarid regions of the QTP, the behavior of  $L_n$  at CD had a dissimilar temporal variation pattern. Since 1996, the  $L_n$  value has continuously increased. From 1993 to 2012,  $L_n$  increased by 2.53 MJ m<sup>-2</sup> day<sup>-1</sup> with an increasing rate of 10.48 MJ m<sup>-2</sup> day<sup>-1</sup> per decade. The mean annual precipitation in CD has declined sharply during the past 20 years, decreasing at a rate of 16.94 mm per decade. Its variation amplitude was about 83.8 % that of mean annual precipitation. This sharp decrease in precipitation may be related to the increased  $L_n$  value.

Among the four regions, the larger  $L_n$  values occurred in the western arid region while smaller  $L_n$  values occurred in the middle semiarid region and southeastern sub-humid region. The  $L_n$  value at SQH in western QTP was greater

than that at GLM, WDL and CD.  $L_n$  generally decreased from west to east. This result is consistent with earlier work conducted in the QTP (Ji et al. 1987). These results are related to geographic location, underlying surface conditions, and local climatic conditions. The differences in surface and local climatic conditions altered the behavior of  $L_n$  in the eastern and western parts of the QTP. SQH is located in the western arid region of the QTP at a higher altitude and a deserted ground surface. Long-wave radiation emitted from the underlying surface of the desert region is large, but the atmospheric counter-radiation under the arid climatic condition is relatively small. Coupled with the region's high altitude and lower atmospheric water vapor content and aerosol particulate concentration, compared to the other stations, the long-wave radiation loss from the ground surface at SQH is relatively large. From west to east,  $L_n$  decreased due to an increase in atmospheric water vapor. The CD station is located in the sub-humid climatic zone of southeastern Tibet, with significant vegetation cover. Precipitation at CD is the highest of the three stations. Due to high atmospheric vapor content and cloudiness, the atmospheric counter-radiation is strong and the long-wave radiation losses from the ground surface are relatively small.

$L_n$  over QTP ranged from 8.99 to 11.09 MJ m<sup>-2</sup> day<sup>-1</sup> with a mean of 9.73 MJ m<sup>-2</sup> day<sup>-1</sup>. This value was greater than those for lower elevations at the same latitude (Ji et al. 1995; Gupta et al. 1999; Smith et al. 2002; Zhang et al. 2010). The value was also much greater than the northern hemisphere mean (4.43 MJ m<sup>-2</sup> day<sup>-1</sup>) and the global mean (4.14 MJ m<sup>-2</sup> day<sup>-1</sup>) (Gupta et al. 1999). Thus, losses due to  $L_n$  on the QTP were much greater than those at the same latitude of lowland regions. The  $L_n$  in all four study regions generally decreased. During the study period,  $L_n$  decreased by 2.10 MJ m<sup>-2</sup> day<sup>-1</sup>, and  $L_n$  declined at a rate of 0.415 MJ m<sup>-2</sup> day<sup>-1</sup> per decade. Trends in increasing precipitation correlated with declines in  $L_n$ . Increased precipitation was a key factor linked to the decline in  $L_n$  over the QTP. During the study period, the annual mean precipitation increased at a rate of 11.7 mm per decade. Atmospheric humidity and amount of cloud cover also increased. With high atmospheric vapor content and cloudiness, the atmospheric counter-radiation is strong and the long-wave radiation loss from the ground surface is relatively small. These factors contribute to increasing downward long-wave radiation. Measurements at WDL showed downward long-wave radiation increasing at a rate of 0.566 MJ m<sup>-2</sup> day<sup>-1</sup> per decade during the past 20 years. The ratio of downward to upward long-wave radiations also increased at a rate of 0.025 per decade. As a result of these factors,  $L_n$  decreased. Low-level cloud cover over the QTP at night had a significant increasing trend from 1961 to 2003, leading to enhanced atmospheric counter-radiation and weakened effective terrestrial radiation

(Dun and Wu 2006). Shi and Liang (2013) noted that downward long-wave radiation across the QTP decreased  $2.5 \text{ Wm}^{-2}$  per decade from 1984 to 2007. On a global scale, daily downward long-wave radiation has increased by  $2.2 \text{ Wm}^{-2}$  per decade from 1973 to 2008 (Wang and Liang 2009). CMIP5 GCMs showed that global  $L_d$  increased by  $1.54 \text{ Wm}^{-2}$  per decade from 1979 to 2005 (Ma et al. 2014).

### Long-term $L_n$ variation and its influence on the thermal state of the ground surface

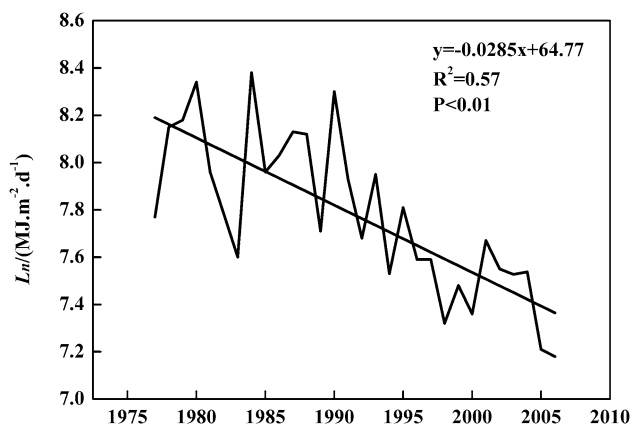
$L_n$  values represent net heat loss from ground surfaces so effects of long-term variation of  $L_n$  on the permafrost and the thermodynamic conditions of the active layer in the QTP region are important. WDL is in the permafrost region of the QTP. Here the radiation climate and surface thermodynamic conditions are representative of the northern part of the QTP, especially the regions between the Kunlun and TGL Mountains (Ji 1999; Jiang and Wang 2000; Zuo et al. 1991). A long history of energy balance observations is available for the WDL station and it is the only station providing comprehensive solar radiation data within the QTP interior. For these reasons, we analyzed WDL  $L_n$  data in relation to the surface temperature.

Figure 3 shows the WDL  $L_n$  series from 1977 to 2006. In the past 30 years,  $L_n$  at WDL has been decreasing. The linear trend was  $-0.285 \text{ MJ m}^{-2} \text{ day}^{-1}/10 \text{ year}$  and this decrease is significant.  $L_n$  decrease occurred primarily in summer and autumn. These declines were  $-0.64$  and  $-0.3 \text{ MJ m}^{-2} \text{ day}^{-1}/10 \text{ year}$ , respectively. In winter and spring, the  $L_n$  declines were  $-0.2$  and  $-0.17 \text{ MJ m}^{-2} \text{ day}^{-1}/10 \text{ year}$ , respectively. The decrease of  $L_n$  in summer and autumn is related to the weather during those seasons. May to October is the WDL rainy season with 94.6 % of the annual precipitation (Li et al. 2005). During this period atmospheric humidity is relatively high, cloudy days are common, and atmospheric counter-radiation is strong, leading to a decrease of  $L_n$ . In

addition, precipitation in the region shows an increasing trend in recent years. Most of the precipitation increase occurs in summer leading to a decrease in the surface net long-wave radiation during this period.

The annual mean daily total amount of  $L_n$  from 1977 to 1986 was as great as  $8.02 \text{ MJ m}^{-2} \text{ day}^{-1}$  (Table 1). From 1987 to 1996,  $L_n$  decreased by  $0.34 \text{ MJ m}^{-2} \text{ day}^{-1}$ , and from 1997 to 2006  $L_n$  decreased by  $0.24 \text{ MJ m}^{-2} \text{ day}^{-1}$  compared with the 1987 to 1996 period. From 1977 to 1993, the variation of  $L_n$  at WDL had an increasing trend but since 1993 it decreased. In the past 30 years the precipitation and  $L_n$  at WDL have had opposite trends. The annual cumulative precipitation increased by 31.3 mm every 10 years, while  $L_n$  declined (the correlation coefficient between precipitation and  $L_n$  was  $-0.65$  at the 0.01 confidence level). The relative humidity in the region also increased. The increase in atmospheric humidity enhanced the atmospheric counter-radiation and partly offset the loss of the surface long-wave radiation and reduced the  $L_n$  values (Prata 2008; Allan 2009; Philipona et al. 2009; Wang and Liang 2009).  $L_n$  trends were also consistent with multi-decadal surface warming trends. With the decrease in  $L_n$ , air temperature has increased about  $1.0 \text{ }^\circ\text{C}$  during the past 30 years (Table 1), and MFD in the seasonal frozen ground decreased about 12.4 cm across the QTP (Li et al. 2009). The ALT increased about 17.7 cm along the Qinghai–Tibetan Highway (Li et al. 2012).

The surface layer temperature cumulative value of the QTP determines the variations of freezing and thawing thickness of the active layer (Ding et al. 2000). The variation of  $L_n$  is closely related to the variation of surface soil temperatures. Therefore, the annual variations of  $L_n$  indirectly reflect the thermodynamic variation characteristics of the active layer. Figure 4a shows the variation curves of  $L_n$  and surface freezing index (DDF) over time during the freezing period at WDL from 1977 to 2006. As the  $L_n$  decreased, the net loss of long-wave energy from the surface also decreased, but the heat used to warm the soil increased. Therefore, the DDF value increased and  $L_n$  had a cooling effect on the ground surface. There was a negative correlation between  $L_n$  and DDF during the freezing period.



**Fig. 3** Inter-annual variation of  $L_n$  at WDL during 1977–2006

**Table 1** Mean values of  $L_n$ , precipitation, relative humidity, and air temperature in different 10-year periods

Parameter	Time period		
	1977–1986	1987–1996	1997–2006
$L_n$ ( $\text{MJ m}^{-2} \text{ day}^{-1}$ )	8.02	7.68	7.44
Precipitation ( $\text{mm year}^{-1}$ )	250.3	286.9	326.4
Relative humidity (%)	56.4	56.6	58.8
Air temperature ( $^\circ\text{C}$ )	$-5.7$	$-5.3$	$-4.7$
MFD (cm)	110.6	101.4	98.2
ALT (cm)	182.7	190.5	200.4

The  $L_n$  series was negatively correlated with freeze-thaw intensity (FTI) (Fig. 4b). Figure 4 shows that although the locations of the crest and trough of the two curves are not exactly matched, their negative correlation is clear. Results of the lag correlation show that the  $L_n$  and the 2-year-lag FTI had significant negative correlation ( $r = 0.66, p < 0.01$ ).  $L_n$  in the WDL region has a significant effect on the soil heat condition.

The radiation climate and surface heat source intensity of the WDL region are characteristic of the northern part of the QTP, but the effects of long-wave radiation variations on the surface heat condition are not understood. To study this mechanism, the  $L_n$  time series of the WDL was compared with the time series of the mean DDF and FTI over the entire QTP during the freezing period. Figure 5 shows that  $L_n$  at the WDL station and the DDF and FTI have opposite trends. As  $L_n$  decreases during the freezing period, the FTI and DDF values increase. A lag correlation analysis of  $L_n$  at the WDL site and the FTI of the QTP surface showed that the  $L_n$  and 2-year-lag FTI also had a significant negative correlation ( $r = -0.57, p < 0.01$ ). Results of the cumulative anomaly of  $L_n$  and FTI of the QTP surface showed that the variations of FTI lag behind the variations

of  $L_n$ . This suggests that the effect of  $L_n$  variations on the surface temperature may be persistent.

### Variations of $L_n/R_s$ and $R_k/R_s$ over the QTP and its adjacent region

Equation (3) shows that in surface radiation balance processes, the energy source is mainly global solar radiation,  $R_s$ . Both  $L_n$  and reflected radiation ( $R_k$ ) are the output energy, and the variations of  $L_n$  and  $R_k$  represent the loss of long-wave and short-wave energy. The surface albedo ( $R_k/R_s$ ) and  $L_n/R_s$  are affected by local climatic and ground surface conditions.

Radiation data from 21 QTP stations and adjacent areas show that the value of  $L_n/R_s$  is clearly larger than that of  $R_k/R_s$  (Table 2). In the northwestern edge of the QTP, the ratio of  $L_n/R_s$  is larger reaching 0.69 in Hami, 0.65 in Hetian, and  $>0.6$  in Dunhuang and Ejinaqi at the northeastern edge of the QTP. On the QTP surface, the  $L_n/R_s$  value is  $>0.4$ . Of the proportion of global solar radiation comprised of reflected radiation, the stations had a mean value  $<0.3$  but the TGL value was greater at 0.338. Table 2 data show that, in the QTP and surrounding regions, the proportion of  $R_s$  attributable to  $L_n$  is 27 % larger than the reflecting

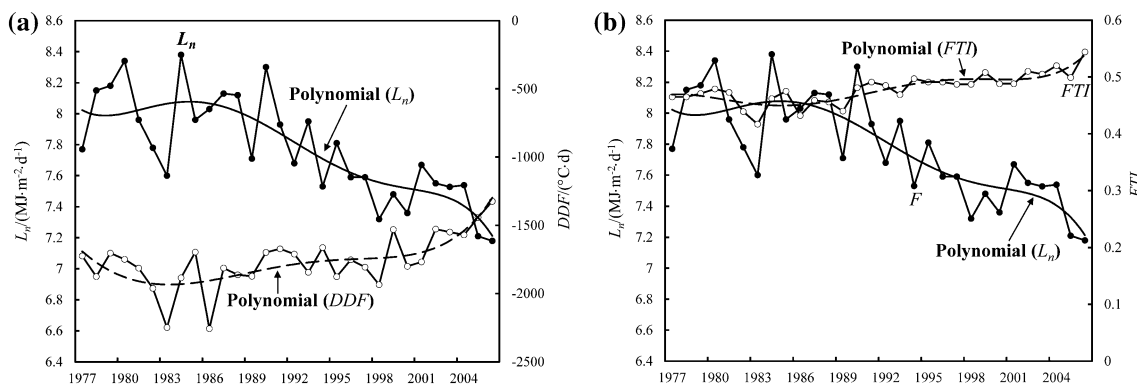


**Fig. 4** Variations of annual mean  $L_n$ , DDF, and FTI at WDL during a 30-year span. **a**  $L_n$  versus DDF; **b**  $L_n$  versus FTI

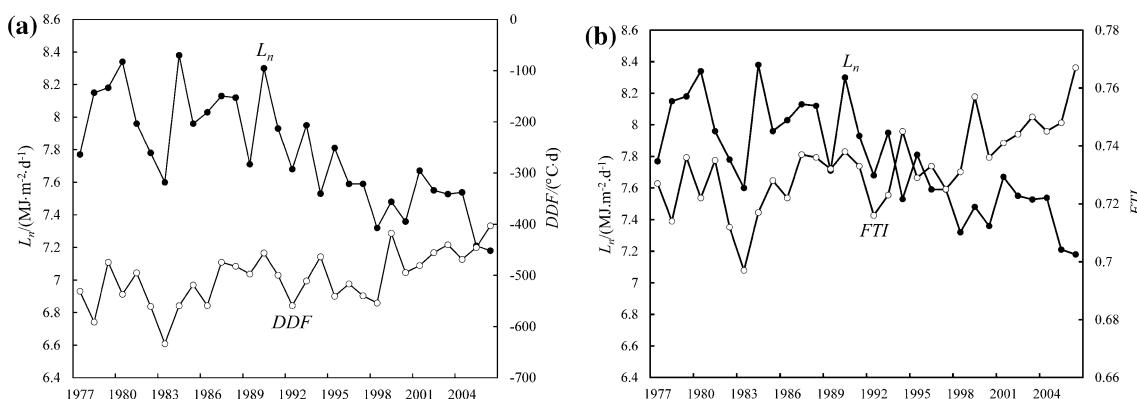


**Fig. 5** The influence of  $L_n$  at WDL on the mean DDF (a) and mean FTI (b) over the entire QTP during a 30-year span

**Table 2**  $R_k/R_s$  and  $F/R_s$  in the QTP and adjacent regions

Site	Latitude (°N)	Longitude (°E)	Elevation (m a.s.l.)	$R_k/R_s$	$L_n/R_s$
Hami	42.82	93.52	737.9	0.242	0.691
Ejinaqi	41.95	101.07	941.3	0.251	0.621
Dunhuang	40.15	94.67	1139.6	0.237	0.622
Kashi	39.47	75.98	1290.7	0.205	0.500
Zhangye	38.93	100.43	1483.7	0.186	0.317
Hetian	37.13	79.93	1374.7	0.235	0.651
Xining	36.72	101.75	2295.2	0.203	0.481
GLM	36.42	94.90	2809.2	0.215	0.523
Lanzhou	36.05	103.88	1518.3	0.156	0.558
XDT	35.43	94.08	4538.0	0.297	0.383
WDL	35.22	93.08	4614.2	0.284	0.510
TGL	33.07	91.94	5100.0	0.338	0.400
SQH	32.50	80.08	4279.3	0.237	0.663
Anduo	32.35	91.10	4801.0	0.131	0.467
Gaize	32.15	84.42	4416.1	0.273	0.476
Ganzi	31.62	100.00	3394.2	0.201	0.394
Naqu	31.48	92.07	4508.0	0.254	0.446
CD	31.15	97.17	3307.1	0.199	0.460
Chengdu	30.67	104.02	507.3	0.131	0.467
Lasa	29.67	91.13	3650.1	0.202	0.492
Kunming	25.02	102.68	1896.8	0.169	0.388

power supporting the findings of Ji et al. (1995, 1999). The  $L_n$  in the QTP and surrounding arid regions, therefore, is an important component of the radiation balance equation. Values of  $L_n/R_s$  also increase with increasing latitude. Table 2 shows that  $L_n/R_s$  values decrease with increasing longitude. Water vapor levels over lower latitude and higher longitude regions are greater than those over the higher latitude and low-longitude region and this may be the major reason for the difference. Comparing the results of this study with previous literature shows that  $L_n/R_s$  over the QTP and its surrounding area is approximately 0.500 indicating that the annual solar radiation loses 50 % as long-wave radiation. This value was much higher than either the global value of about 0.26 (Gupta et al. 1999) or lowland areas at the same latitude (Ji et al. 1995, 2003). High altitude, less atmospheric water vapor, and relatively less precipitation may all contribute to the higher  $L_n/R_s$  ratio over the QTP and surrounding regions.

### Effect of $L_n/R_s$ on the surface layer soil temperature in the QTP region

The effects of  $L_n$  of the QTP surface and surface reflected radiation on the surface temperature were studied using the following equation:  $GT = f(L_n/R_s, R_k/R_s)$ , where GT denotes soil temperature. We considered two factors,  $L_n/R_s$  and  $R_k/R_s$ , to quantitatively analyze effects on the surface temperature.

We used data from six stations in different QTP regions to derive the following regression equation:

$$GT = a + b \times L_n/R_s + c \times R_k/R_s \quad (6)$$

where GT represents the soil temperature at 0-, 2-, or 5-cm depth, and  $a$ ,  $b$ , and  $c$  are regression coefficients (corresponding correlation coefficients and regression coefficients are given in Table 3). Table 3 shows that on the monthly scale, the two factors have a close relation with the surface temperature. The partial correlation coefficient of  $L_n/R_s$  is larger than  $R_k/R_s$ , and the multiple correlation coefficients of the six stations are  $>0.71$  and passes the  $F$  test at the 0.01 confidence level.

The regression coefficients  $b$  and  $c$  of Eq. (6), given in Table 3, are negative and indicate that the two factors have negative impacts on the surface temperature. This is consistent with the physical mechanism of  $L_n$  and  $R_k$ .  $L_n$  represents the loss of long-wave radiation from the ground surface, so the energy loss from the surface lowers the surface temperature. Higher surface albedo reduces the absorption of solar short-wave radiation and also contributes to cooling the surface. Thus, the correlation analysis results have a corresponding physical significance.

The analysis demonstrates that the  $L_n/R_s$  value is larger than the  $R_k/R_s$  value in the QTP region. Among the six stations studied, the absolute value of the coefficient  $b$  is larger than the coefficient  $c$ , suggesting that the cooling effect of  $L_n$  is greater than that of the  $R_k$ . At the WDL



**Table 3** Correlation coefficients and regression coefficients of Eq. (6)

Site	Sample number	PCC		MCC	F test	Regression coefficient		
		$r(L_n/R_s)$	$r(R_k/R_s)$			$a$	$b$	$c$
TGL	55	0.982	0.831	0.868	79.17	22.23	-45.69	-14.70
WDL	72	0.990	0.987	0.945	290.12	40.36	-49.78	-65.94
XDT	50	0.987	0.964	0.919	127.92	22.90	-37.26	-28.15
GLM	120	0.992	0.456	0.82	119.53	58.88	-90.24	-14.08
SQH	120	0.983	0.811	0.712	60.24	59.04	-63.49	-46.38
CD	120	0.99	0.51	0.93	381.4	38.69	-56.65	-9.25

station, the absolute value of coefficient  $b$  was smaller than coefficient  $c$ , but the  $L_n/R_s$  value was almost two times the  $R_k/R_s$  value which would act to partly offset the surface cooling effect due to the small value of coefficient  $b$ .

Figure 6 shows soil temperatures at six stations calculated using Eq. (6). Some discrepancies exist but the

equation reasonably simulates the soil temperature variation trend in the surface layer. The regression equation can adequately describe the surface temperature variations and can be used to analyze the contributions of equation

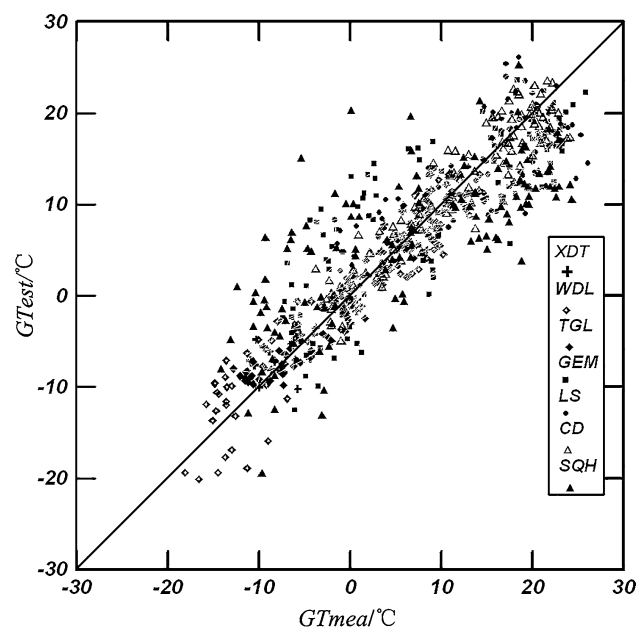


**Fig. 6** Comparison of calculated soil temperatures at seven research sites

**Table 4** Contributions of mean  $L_n/R_s$  and  $R_k/R_s$  to topsoil temperature at different sites

Site	Contribution (°C)		Contribution (%)	
	$L_n/R_s$	$R_k/R_s$	$L_n/R_s$	$R_k/R_s$
TGL	-18.2	-4.8	79.1	20.9
WDL	-22.0	-19.2	53.4	46.7
XDT	-14.5	-8.8	62.2	37.8
GLM	-47.2	-3.0	94.0	6.0
SQH	-42.0	-11.0	79.2	20.8
CD	-26.0	-1.8	93.5	6.5

**Table 5** Contributions of  $L_n/R_s$  and  $R_k/R_s$  to decreasing the ground surface temperature

$\Delta x_i$	TGL		WDL		XDT	
	$L_n/R_s$	$R_k/R_s$	$L_n/R_s$	$R_k/R_s$	$L_n/R_s$	$R_k/R_s$
0.01	-18.69	-4.97	-22.45	-19.85	-14.87	-9.04
0.02	-19.14	-5.12	-22.95	-20.51	-15.24	-9.32
0.03	-19.60	-5.26	-23.45	-21.17	-15.61	-9.60
0.04	-20.06	-5.41	-23.94	-21.83	-15.98	-9.88
0.05	-20.51	-5.56	-24.44	-22.49	-16.36	-10.16
0.06	-20.97	-5.70	-24.94	-23.14	-16.73	-10.44
0.07	-21.43	-5.85	-25.44	-23.80	-17.10	-10.73
0.08	-21.89	-6.00	-25.94	-24.46	-17.47	-11.01
0.09	-22.34	-6.14	-26.43	-25.12	-17.85	-11.29
0.10	-22.80	-6.29	-26.93	-25.78	-18.22	-11.57
0.11	-23.26	-6.44	-27.43	-26.44	-18.59	-11.85
0.12	-23.71	-6.59	-27.93	-27.10	-18.97	-12.13
0.13	-24.17	-6.73	-28.42	-27.76	-19.34	-12.41
0.14	-24.63	-6.88	-28.92	-28.42	-19.71	-12.70
0.15	-25.08	-7.03	-29.42	-29.08	-20.08	-12.98
0.16	-25.54	-7.17	-29.92	-29.74	-20.46	-13.26
0.17	-26.00	-7.32	-30.42	-30.40	-20.83	-13.54
0.18	-26.45	-7.47	-30.91	-31.06	-21.20	-13.82
0.19	-26.91	-7.61	-31.41	-31.72	-21.57	-14.10
0.20	-27.37	-7.76	-31.91	-32.38	-21.95	-14.38
0.21	-27.83	-7.91	-32.41	-33.04	-22.32	-14.67
0.22	-28.28	-8.06	-32.90	-33.70	-22.69	-14.95
0.23	-28.74	-8.20	-33.40	-34.35	-23.06	-15.23
0.24	-29.20	-8.35	-33.90	-35.01	-23.44	-15.51
0.25	-29.65	-8.50	-34.40	-35.67	-23.81	-15.79
0.26	-30.11	-8.64	-34.90	-36.33	-24.18	-16.07
0.27	-30.57	-8.79	-35.39	-36.99	-24.55	-16.36
0.28	-31.02	-8.94	-35.89	-37.65	-24.93	-16.64
0.29	-31.48	-9.08	-36.39	-38.31	-25.30	-16.92
0.30	-31.94	-9.23	-36.89	-38.97	-25.67	-17.20

variables to the decrease in surface temperature. We used regression coefficients corresponding to the  $L_n/R_s$  and  $R_k/R_s$  at various stations to evaluate their contributions to the surface layer soil temperature variations. The results are shown in Table 4. The contribution of  $L_n/R_s$  to lowering the ground surface temperature at various sites is >50 %. At the GLM, SQH, and CD stations, the contribution of  $L_n/R_s$  to the surface temperature drop is much greater than that of  $R_k/R_s$ . The mean contribution is 24 °C greater than the contribution of  $R_k/R_s$ , representing a contribution greater than 78 %. At the TGL, WDL, and XDT stations, the contribution of  $R_k/R_s$  to lowering the ground surface temperature increased with altitude. This is because atmospheric water vapor decreases with the increased altitude. Atmospheric water vapor content strongly affects the declining long-wave radiation trend. Decreased water vapor content results in a decrease in long-wave radiation. As a result,  $L_n$  loss from the surface increases and its corresponding proportion in the global solar radiation also increases.

The WDL station was anomalous compared with the TGL and XDT stations. This was related to the underlying surface and local climate of the WDL area. The observation area of the WDL station has almost no vegetation. The surface area soils are relatively dry and sandy. The weather during the WDL rainy season is particularly variable (Wang 1983). There are as many as 172.9 snowfall days per year and up to 84 days of snow cover (Shao and Zhang 1998), which might be a reason for the anomaly in the region.

To study the temperature-lowering effect of  $L_n/R_s$  and  $R_k/R_s$  variations on the surface soil layer, we used the following equation to evaluate the contribution of the increased  $L_n/R_s$  and  $R_k/R_s$  to lowering the surface soil layer temperature:

$$GT = c_i \times (\bar{x}_i + \Delta x_i) \quad (i = 1, 2) \quad (7)$$

where 1 and 2 represent  $L_n/R_s$  and  $R_k/R_s$ , respectively;  $c_i$  is the coefficient of the two factors corresponding to Eq. (6);  $\bar{x}_i$  is the mean value of the observation series of the two factors; and  $\Delta x_i$  is the increment. The calculated results are given in Table 5 and Fig. 7. With the same increment at the TGL and XDT stations, the contribution of  $L_n/R_s$  variations to lowering the topsoil temperature is greater than that of  $R_k/R_s$ . As the two factors increase by 1 %, the contribution of  $L_n/R_s$  to the topsoil temperature drop is 18.8 °C greater than that of the  $R_k/R_s$ . The variation characteristics at the WDL station are different from those at the TGL and XDT stations. As the average  $L_n/R_s$  increases by 17 %, the topsoil temperature-cooling effect of  $L_n/R_s$  is lower than the  $R_k/R_s$ , but the difference is slight. The contribution of  $L_n$  in the WDL region to surface temperature variation is nearly 2.8 °C larger than the contribution of the reflecting power.

However, as  $L_n/R_s$  and  $R_k/R_s$  increase, the difference between the two gradually decreases. After increasing to a certain degree, the topsoil temperature-cooling effect of the surface reflecting power is greater than the  $L_n$  (in the case of solid precipitation). The contribution of  $L_n/R_s$  to the surface temperature decrease in the QTP region varies due to regional surface characteristics and local climates. In the QTP, the surface net long-wave radiation is more important in lowering the surface temperature than the surface albedo.

## Conclusions

$L_n$  in the QTP is an important output item in the surface energy exchange processes, and it has important effects on physical processes, such as surface radiation balance, underlying surface thermodynamic conditions, and land-atmosphere energy exchange. The following conclusions were drawn:

1. The behavior of  $L_n$  in the QTP varied regionally.  $L_n$  in the arid western and northern parts of the QTP was greater than in the sun-humid southeastern region.  $L_n$  values ranged from 8.99 to 11.09 MJ m<sup>-2</sup> day<sup>-1</sup> with a mean of 9.73 MJ m<sup>-2</sup> day<sup>-1</sup> and decreased at a rate of 0.415 MJ m<sup>-2</sup> day<sup>-1</sup> per decade. At the same latitude,  $L_n$  values at high elevations were significantly greater than those at lower elevations.  $L_n$  values were also significantly greater than those for hemispheric and global scales. Underlying surface characteristics and local climatic conditions influenced the spatial pattern of  $L_n$ .
2.  $L_n$  affects the formation and duration of the surface freezing index (DDF) in the surface soil layer during the freezing period. The DDF significantly increases as  $L_n$  decreases during the freezing period. The  $L_n$  in the WDL area and the FTIs in that region and the QTP surface are negatively correlated so that as  $L_n$  increases, FTI decreases. The correlation between  $L_n$  and the 2-year-lag FTI is stronger suggesting that the effects of  $L_n$  on surface thermodynamic conditions are persistent.
3.  $L_n$  was negatively correlated ( $r = -0.65$ ) with variation in regional precipitation.
4. The proportion of  $L_n$  within the  $R_s$  was greater than that within the  $R_k$  and it constitutes the largest fraction of the energy output of the surface radiation balance.
5. The spatial distribution pattern of  $L_n/R_s$  varies among QTP regions. Highest values occur in the western areas and the lowest values occur at the northeastern edge.  $L_n/R_s$  decreases with decreasing longitude but increases with latitude.  $L_n/R_s$  values in the QTP were

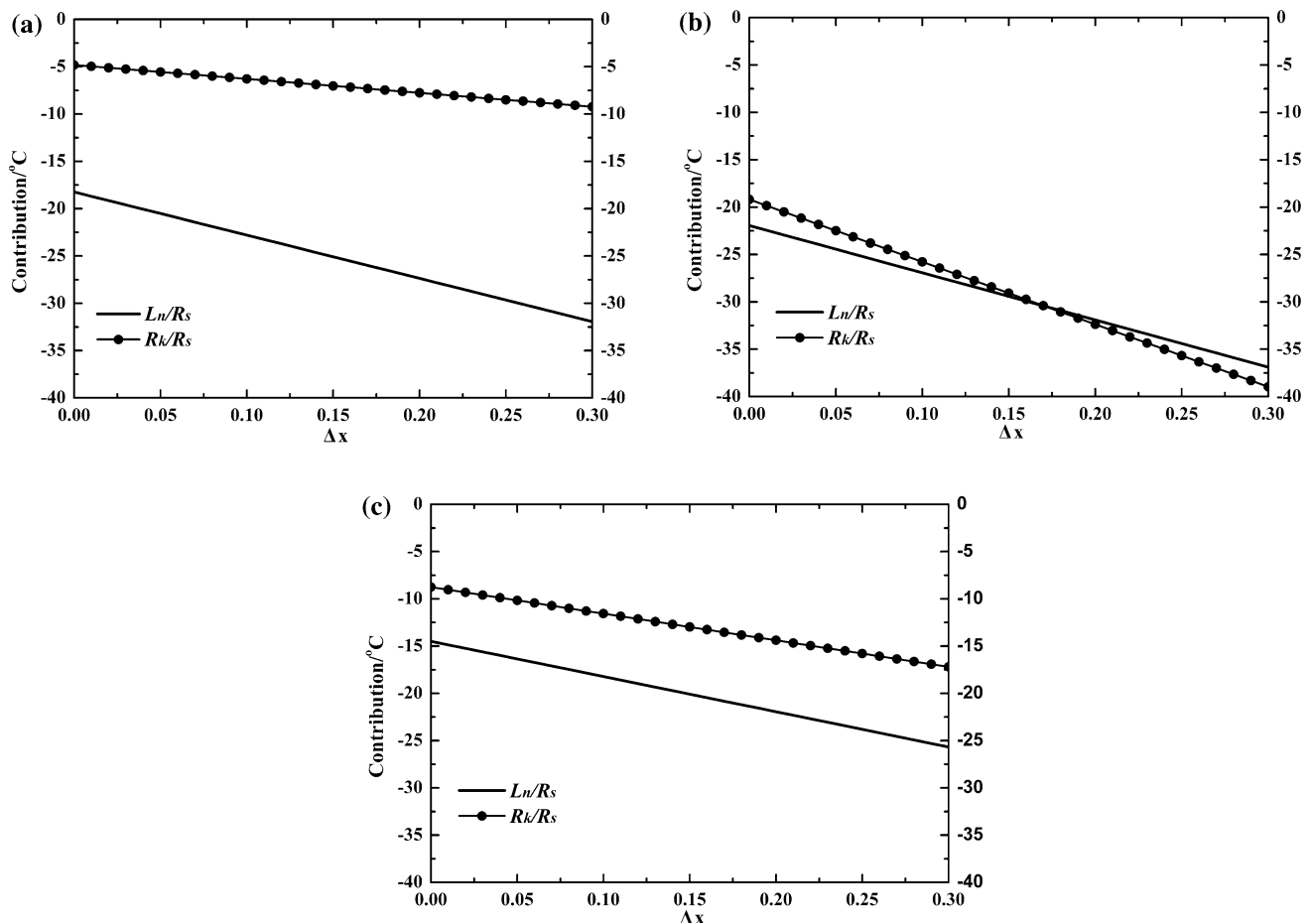


**Fig. 7** Contributions of  $L_n/R_s$  and  $R_k/R_s$  to lowering the ground surface temperature at **a** TGL, **b** WDL, **c** TGL

significantly greater than global means and also greater than values in lowland areas of China.

6.  $L_n/R_s$  and  $R_k/R_s$  ratios in the QTP region represent the loss of surface energy and lowering of surface temperatures. The magnitude of the surface temperature-cooling effects varies with geographic location and climatic conditions but, in general, the surface temperature-lowering effects of  $L_n/R_s$  exceed those of  $R_k/R_s$ .

**Acknowledgments** This study is financially supported by National Major Scientific Project of China “Cryospheric Change and Impacts Research” (2013CBA01803), the National Natural Sciences Foundation of China (Grant Nos. 41271081, 41271086), and the Hundred Talents Program of the Chinese Academy of Sciences (Grant Nos. 51Y251571, 51Y551831).

**References**

Allan RP (2009) Examination of relationships between clear-sky longwave radiation and aspects of the atmospheric hydrological cycle in climate models, reanalyses, and observations. *J Clim* 22:3127–3145

Ding YJ, Ye BS, Liu SY, Shen YP, Wang SL, Yang MX (2000) Observational study on the permafrost hydrological processes in large scale on the Tibetan Plateau. *Chin Sci Bull* 45(2):208–214

Dun AM, Wu GX (2006) Change of cloud amount and the climate warming on the Tibetan plateau. *Geophys Res Lett* 33:L22704. doi:10.1029/2006GL027946

Frauenfeld OW, Zhang T, McCreight JL (2007) Northern hemisphere freezing/thawing index variations over the twentieth century. *Int J Climatol* 27:47–63

Gao GD, Lu YR (1982) Land surface radiation balance and heat balance in China. Science Press, Beijing, pp 63–86

Gupta SK, Ritchey NA, Wilber AC, Whitlock CH, Gibson GG, Stackhouse PW Jr (1999) A climatology of surface radiation budget derived from satellite data. *J Clim* 12(8):2691–2710. doi:10.1175/1520-0442

Iziomon MG, Mayer H, Wicke W, Matzarakis A (2001) Radiation balance over low-lying and mountainous areas in south-west Germany. *Theor Appl Climatol* 68:219–231. doi:10.1007/s007040170047

Jacovides CP, Kallos GB, Steven MD (1993) Spectral band resolution of solar radiation in Athens, Greece. *Int J Climatol* 13(6):689–697

Ji GL (1985) The relationship between the radiation and climate in Qinghai-Xizang Plateau during August 1982 to July 1983. *Plateau Meteorol* 4(4, supplement):10–20

Ji GL (1997) Observation and research on the radiation budget in the region of Qinghai–Tibetan Plateau. Research on climate change and its impact in China. China Meteorological Press, Beijing, pp 124–131

- Ji GL (1998) Radiation budget in the region of plateau. Climate change and its impact on the environment on the Qinghai–Tibetan Plateau in modern time. Guangzhou Science and Technology Press, Guangzhou, pp 1–32
- Ji GL (1999) Advances in the energy budget observation experiment over the Qinghai–Tibetan Plateau. *Plateau Meteorol* 18(3):333–340
- Ji GL (2003) Observation experiment on surface radiation budget and heat source on the plateau. Formation and Evolution of the Qinghai–Tibetan Plateau. Hebei Science and Technology Press, Shijiazhuang, pp 120–129
- Ji GL, Yao LC, Yuan FM (1986) Characteristics of surface and atmospheric heating fields over Qinghai–Tibetan Plateau during the winter in 1982. *Sci Chin Ser B* 29(8):876–888
- Ji GL, Jiang H, Zhang SF (1987) The computation and some distribution characteristics of effective radiation over the Qinghai–Tibetan Plateau and its adjacent areas. *Plateau Meteorol* 6(2):141–149
- Ji GL, Zhong Q, Shen ZB (1989) Advances in observation and research of the surface heat source over the Qinghai–Tibetan Plateau. *Plateau Meteorol* 8(2):127–132
- Ji GL, Jiang H, Lu LZ (1995) Features of long-wave radiation on the Qinghai–Tibetan Plateau. *Plateau Meteorol* 14(4):451–458
- Ji GL, Jiang H, Zou JL (1996) Features of ground radiation budget in the area of Wudaoliang on the Qinghai–Tibetan Plateau. Annual of researches on the formation, evolution, environmental change and ecosystem of Qinghai–Tibetan Plateau (1995). Science Press, Beijing, pp 211–217
- Ji GL, Zou JL, Lu LZ (1997) The seasonal variation of surface heating field over the Northern Qinghai–Tibetan Plateau. *Plateau Meteorol* 16(1):1–9
- Jiang H, Wang KL (2000) Analysis of the surface temperature over Qinghai–Tibetan Plateau from satellite. *Plateau Meteorol* 19(3):328–330
- Li R, Ji GL, Yang W (2005) Retrieve aerosol optical information from atmospheric broad-band transmittance on clear sky. *Acta Energe Sol Sin* 26(2):150–156
- Li R, Ji GL, Yang W, Zhao JQ (2006) Parameterization of effective radiation over the Qinghai–Tibetan Plateau. *Acta Energe Sol Sin* 27(3):274–278
- Li R, Zhao L, Ding YJ, Shen YP, Du EJ, Liu GY (2009) The climatic characteristics of the maximum seasonal frozen depth in the Tibetan Plateau. *J Glaciol Geocryol* 31(6):1050–1056
- Li R, Zhao L, Ding YJ, Wu TH, Xiao Y, Du EJ, Liu GY, Qiao YP (2012) Temporal and spatial variations of the active layer along the Qinghai–Tibet highway in a permafrost region. *Chin Sci Bull* 57(35):4609–4616
- Ma Q, Wang KC, Wild M (2014) Evaluations of atmospheric downward longwave radiation from 44 coupled general circulation models of CMIP5. *J Geophys Res Atmos* 119:4486–4497. doi:10.1002/2013JD021427
- Nelson FE, Anisimov OA (1993) Permafrost zonation in Russia under anthropogenic climate change. *Permafr Periglac Process* 4(2):137–148
- Nelson FE, Outcalt SI (1987) A computational method for prediction and regionalization of permafrost. *Arct Alp Res* 19(3):279–288
- Niemelä N, Räisänen P, Savijärvi H (2001) Comparison of surface radiative flux parameterizations. Part I: long wave radiation. *Atmos Res* 58(1):1–18
- Philipona R, Behrens K, Ruckstuhl C (2009) How declining aerosols and rising greenhouse gases forced rapid warming in Europe since the 1980s. *Geophys Res Lett* 36:L02806
- Prata F (2008) The climatological record of clear-sky longwave radiation at the Earth's surface: evidence for water vapour feedback? *Int J Remote Sens* 29:5247–5526
- Ruckstuhl C, Philipona R, Behrens K, Coen MC, Dürr B, Heimo A, Mätzler C, Nyeki S, Ohmura A, Vuilleumier L, Weller M, Wehrli C, Zelenka A (2008) Aerosol and cloud effects on solar brightening and the recent rapid warming. *Geophys Res Lett* 35:L12708
- Shao HY, Zhang HL (1998) Climatic features in the source regions of the Yangtze and Yellow rivers. *Qinghai Environ* 8(2):68–72
- Shi QQ, Liang SL (2013) Characterizing the surface radiation budget over the Tibetan Plateau with ground-measured, reanalysis, and remote sensing data sets. 2. Spatiotemporal analysis. *J Geophys Res Atmos* 118:8921–8934. doi:10.1002/jgrd.50719
- Smith GL, Wilber AC, Gupta SK, Stackhouse PW (2002) Surface radiation budget and climate classification. *J Clim* 15(10):1175–1188
- Sun ZA, Weng DM (1986) Climatological calculation and distributional features of effective radiation over China (Part II): empirical computation method and distribution features. *J Nanjing Institute Meteorol* 4:335–347
- Wacker S, Gröbner J, Hocke K, Kämpfer N, Vuilleumier L (2011) Trend analysis of surface cloud-free downwelling long-wave radiation from four Swiss sites. *J Geophys Res Atmos* 116:D10104. doi:10.1029/2010JD015343
- Wang GZ (1983) Essay about the climate of Wudaoliang. *Meteorol Monthly* 2:27
- Wang KC, Liang SL (2009) Global atmospheric downward longwave radiation over land surface under all-sky conditions from 1973 to 2008. *J Geophys Res Atmos* 114(D19101):D19101. doi:10.1029/2009JD011800
- Weng DM, Feng YH (1984) Feature analysis of effective terrestrial radiation and atmospheric counter radiation in summer on the Qinghai–Tibetan Plateau. *Chin Sci Bull* 13:796–799
- Weng DM, Chen WL, Shen JC (1984) A discussion on the computation method for the climate from the total quantity of effective radiation at arbitrary periods on Qinghai–Tibetan Plateau. *Plateau Meteorol* 3(1):73–82
- Wu TH, Wang QX, Zhao L, Batkhisig O, Watanabe M (2011) Observed trends in surface freezing/thawing index over the period 1987–2005 in Mongolia. *Cold Reg Sci Technol* 69(1):105–111
- Zhang XC, Gu S, Zhao XQ, Cui XY, Zhao LL, Xu SX, Du MY, Jiang S, Yb G, Ma C, Tang YH (2010) Radiation partitioning and its relation to environmental factors above a meadow ecosystem on the Qinghai–Tibetan Plateau. *J Geophys Res Atmos* 115:D10106. doi:10.1029/2009JD012373
- Zhao L, Li R, Ding YJ (2008) Simulation on the soil water-thermal characteristics of the active layer in Tanggula Range. *J Glaciol Geocryol* 30(6):930–937
- Zheng D, Zhang RZ, Yang QY (1979) On the natural zonation in the Qinghai–Xizang Plateau. *Acta Geogrphica Sinica* 34(1):1–11
- Zhou YH (1984a) An empirical method for estimating surface long-wave radiation exchanges in the Qinghai–Tibetan Plateau. *Acta Geogr Sin* 39(2):148–162
- Zhou YH (1984b) A study on the net long-wave radiation over the Qinghai–Tibetan Plateau in summer by use of satellite cloud pictures. *Plateau Meteorol* 3(1):60–72
- Zhou YH, Li YH, Zuo DK (1964) Comparison of several radiation charts. *Acta Meteorol Sin* 34(2):135–145
- Zhou SZ, Zhang RR, Zhang C (1990) Meteorology and climatology, 2nd edn. Higher Education Press, Beijing, pp 40–42
- Zhou YW, Qiu GQ, Guo DX, Cheng GD (2000) China's frozen ground. Science Press, Beijing, pp 1–62
- Zuo DK, Chen JS, Li YH, Zhou YH (1965) Radiation balance of the “earth-atmosphere” system and the atmosphere over eastern Asia. *Acta Geogr Sin* 31(2):100–112
- Zuo DK, Zhou YH, Xiang YQ (1991) The earth's surface radiation research. Science Press, Beijing, pp 37–49